APPLICATION OF DFT-DERIVED RELATIONSHIPS BETWEEN CHEMICAL ENVIRONMENT AND ^{29}SI NUCLEAR MAGNETIC RESONANCE SPECTROSCOPY TO DETERMINE STRUCTURE IN SILICON OXYCARBIDE CERAMICS

by

JOHN PAUL NIMMO II

THESIS

Submitted in partial fulfillment of the requirements
for the degree of Master of Science in Chemistry at
The University of Texas at Arlington
May, 2017

Arlington, Texas

Supervising Committee:

Peter Kroll, Supervising Professor
Frederick MacDonnell
Bradley Pierce

ABSTRACT/INTRODUCTION

Silicon oxycarbide (SiCO) is an amorphous ceramic material widely used in industrial applications, for its useful electronic and biologically-compatible properties.[1-3] SiCO is resistant to crystallization, remaining amorphous even above temperatures at which amorphous SiO_2 would crystallize. Though silica (SiO_2) and silicon carbide (SiC) are almost immiscible, it is useful to consider the material as a phase composition of these along with carbon, according to the formula below. The first two terms in braces can be considered as being the "SiCO glass" into which a third term representing excess or "free" carbon is incorporated as graphite-like nano-flakes and bands.

$$SiC_xO_y = \left\{\frac{y}{2}SiO_2 + \left(1 - \frac{y}{2}\right)SiC\right\} + \left(x + \frac{y}{2} - 1\right)C.$$

Since these components are not able to be mixed, SiCO is typically made using a pyrolytic conversion from molecular or polymeric precursors. [4-6] This process is often monitored using ^{29}Si solid-state nuclear magnetic resonance spectroscopy (SS-NMR, or simply NMR)[7], because the changes in chemical bonding are observable through changes in the NMR signal. Clearly defined peaks can be seen for each type of $\{Si\}C_xO_{4-x}$ tetrahedra present in the material. Differences in the chemical bonding environment affect the shielding of the nucleus, changing where the resulting signal appears in the spectrum.[8] The area under these peaks can be integrated and used as a measure of the relative population of each chemical bonding environment. As the process of pyrolysis progresses the bonding environment around Si changes and so the shapes and ratios of these peaks shift accordingly.[9]

The precise mechanism of the interface between the free carbon and the host glass remains a topic of debate regarding SiCO. Though plausible models have been proposed in literature, supported by different infrared and X-ray spectroscopic data,[10,11] none provide direct

evidence regarding the nature of any chemical bonding or interaction between free carbon and silicon in the bulk glass. Recently, computational modeling has shown that there is a large energetic penalty for a bonding interaction between graphitic carbon and glassy SiCO.[12] There has, however been no direct investigation to search for the nature of this interface.

Computer modeling of both structure and spectroscopy has proven to be an invaluable tool in the examination of materials and their properties.[13-16] Hundreds of chemical systems can be constructed, analyzed, and compared to experimental results, allowing the exploration of environments and effects which might be difficult to access experimentally.[17-21] For this work, models were generated using a modified Wooten-Winer-Weaire[22] (WWW) method to provide a multitude of chemical environments to investigate. The use of density functional theory (DFT) along with the gauge-including projector augmented wave (GIPAW) method[23] facilitates the calculation of NMR signals and parameters for the models. A small piece of custom software is used to extract precise structural information such as angles and distances between atoms from each model as well as the corresponding computed NMR chemical shift for each silicon atom.

Structural-chemical relationships in SiCO ceramics are investigated using these methods in an attempt to increase the amount of information that it is possible to extract from an experimental NMR spectrum. Nearby structural features within the model structures – the Si—O—Si tetrahedral bonding angles around every silicon atom are correlated with the computed NMR chemical shift for that atom. This gives a linear function relating the average Si—O—Si bonding angle around a central Si atom, for each SiC_xO_{4-x} center (for $0 \leq x \leq 3$). These angular correlation functions can in turn be applied to experimental NMR data to extract information about the distribution of angles within the material. Furthermore, appropriate models are analyzed in order to discern the differences between silicon bound to 3-connected (sp^2-bonded)

carbon bound to silicon versus 4-connected (sp^3-bonded) carbon bound to silicon. Models which compared systems with free carbon chemically bound to the glass with models where the free carbon is completely disconnected are also included. Therefore experimental spectra can be analyzed to extract the distribution of Si—O—Si angles and to search for evidence of bonding between graphitic carbon and Si atoms in the host glass.

REFERENCES

1. Meier, A.; Weinberger, M.; Pinkert, K.; Oschatz, M.; Paasch, S.; Giebeler, L.; Althues, H.; Brunner, E.; Eckert, J.; Kaskel, S. Silicon Oxycarbide-Derived Carbons from a Polyphenylsilsequioxane Precursor for Supercapacitor Applications. *Microporous Mesoporous Mater.* **2014**, 188, 140−148.
2. Konno, H.; Kasashima, T.; Azumi, K. Application of Si−C−O Glass-Like Compounds as Negative Electrode Materials for Lithium Hybrid Capacitors. *J. Power Sources* **2009**, 191, 623−627.
3. Zhuo, R.; Colombo, P.; Pantano, C.; Vogler, E. A. Silicon Oxycarbide Glasses for Blood-Contact Applications. *Acta Biomater*. **2005**, 1, 583−589.
4. Baird, J. D.; Taylor, J. Reaction between Silica and Carbon and the Activity of Silica in Slag Solution. *Trans. Faraday Soc*. **1958**, 54, 526−539.
5. Klinger, N.; Strauss, E. L.; Komarek, K. L. Reactions between Silica and Graphite. *J. Am. Ceram. Soc*. **1966**, 49, 369−375.
6. Walter, S.; Soraru, G. D.; Bréquel, H.; Enzo, S. Microstructural and Mechanical Characterization of Sol Gel-Derived Si−O−C Glasses. *J. Eur. Ceram. Soc*. **2002**, 22, 2389−2400.
7. Eckert, H.; Ribeiro, S. L.; Santagneli, S.; Nalin, M.; Poirier, G.; Messaddeq, Y. Glasses on the Nanoscale. In *Springer Handbook of Nanomaterials*; Vajtai, R., Ed.; Springer: Berlin, **2013**; pp 665−692.
8. Bois, L.; Maquet, J.; Babonneau, F.; Bahloul, D. Structural Characterization of Sol-Gel Derived Oxycarbide Glasses. 2. Study of the Thermal Stability of the Silicon Oxycarbide Phase. *Chem. Mater*. **1995**, 7, 975−981.
9. Bréquel, H.; et al. Systematic Structural Characterization of the High-Temperature Behavior of Nearly Stoichiometric Silicon Oxycarbide Glasses. *Chem. Mater*. **2004**, 16, 2585−2598.
10. Widgeon, S. J.; Sen, S.; Mera, G.; Ionescu, E.; Riedel, R.; Navrotsky, A. ^{29}Si and ^{13}C Solid-State NMR Spectroscopic Study of Nanometer-Scale Structure and Mass Fractal Characteristics of Amorphous Polymer Derived Silicon Oxycarbide Ceramics. *Chem. Mater*. **2010**, 22, 6221−6228.
11. Saha, A.; Raj, R.; Williamson, D. L. A Model for the Nanodomains in Polymer-Derived SiCO. *J. Am. Ceram. Soc*. **2006**, 89, 2188−2195.
12. Kroll, P. Searching Insight into the Atomistic Structure of SiCO Ceramics. *J. Mater. Chem*. **2010**, 20, 10528−10534.
13. Charpentier, T.; Kroll, P.; Mauri, F. First-Principles Nuclear Magnetic Resonance Structural Analysis of Vitreous Silica. *J. Phys. Chem. C* **2009**, 113, 7917−7929.
14. Ferlat, G.; Charpentier, T.; Seitsonen, A. P.; Takada, A.; Lazzeri, M.; Cormier, L.; Calas, G.; Mauri, F. Boroxol Rings in Liquid and Vitreous B_2O_3 from First Principles. *Phys. Rev. Lett.* **2008**, 101, 065504.
15. Pedone, A.; Charpentier, T.; Menziani, M. C. The Structure of Fluoride-Containing Bioactive Glasses: New Insights from First-Principles Calculations and Solid State NMR Spectroscopy. *J. Mater. Chem*. **2012**, 22, 12599−12608.
16. Profeta, M.; Mauri, F.; Pickard, C. J. Accurate First Principles Prediction of ^{17}O NMR Parameters in SiO_2: Assignment of the Zeolite Ferrierite Spectrum. *J. Am. Chem. Soc*. **2002**, 125, 541−548.
17. Hanna, J. V.; Smith, M. E. Recent Technique Developments and Applications of Solid State NMR in Characterising Inorganic Materials. *Solid State Nucl. Magn. Reson*. **2010**, 38, 1−18.
18. Charpentier, T.; Menziani, M. C.; Pedone, A. Computational Simulations of Solid State NMR Spectra: A New Era in Structure Determination of Oxide Glasses. *RSC Adv*. **2013**, 3, 10550−10578.

19. Ashbrook, S. E.; Dawson, D. M. Exploiting Periodic First-Principles Calculations in NMR Spectroscopy of Disordered Solids. *Acc. Chem. Res*. **2013**, 46, 1964−1974.
20. Pallier, C.; Leyssale, J.-M.; Truflandier, L. A.; Bui, A. T.; Weisbecker, P.; Gervais, C.; Fischer, H. E.; Sirotti, F.; Teyssandier, F.; Chollon, G. Structure of an Amorphous Boron Carbide Film: An Experimental and Computational Approach. *Chem. Mater*. **2013**, 25, 2618−2629.
21. Pedone, A.; Gambuzzi, E.; Menziani, M. C. Unambiguous Description of the Oxygen Environment in Multicomponent Aluminosilicate Glasses from ^{17}O Solid State NMR Computational Spectroscopy. *J. Phys. Chem. C* **2012**, 116, 14599−14609.
22. Wooten, F.; Winer, K.; Weaire, D. Computer Generation of Structural Models of Amorphous Si and Ge. *Phys. Rev. Lett.* **1985**, 54, 1392−1395.
23. Pickard, C. J.; Mauri, F. All-Electron Magnetic Response with Pseudopotentials: NMR Chemical Shifts. *Phys. Rev. B* **2001**, 63, 245101.

TABLE OF CONTENTS

THE JOURNAL OF PHYSICAL CHEMISTRY C

Article

pubs.acs.org/JPCC

First-Principles Calculations and Analysis of ^{29}Si Nuclear Magnetic Resonance Chemical Shifts in Silicon Oxycarbide Ceramics

John P. Nimmo, II and Peter Kroll*

Department of Chemistry and Biochemistry, The University of Texas at Arlington, 700 Planetarium Place, Arlington, Texas 76019, United States

ABSTRACT: We calculate ^{29}Si NMR chemical shifts for silicon atoms in different chemical environments observed in amorphous silicon oxycarbide ceramics using a library of optimized structural models and the gauge-including projector augmented wave (GIPAW) method. For each type of mixed tetrahedral environment, $\{Si\}O_4$, $\{Si\}O_3C$, and $\{Si\}O_2C_2$, we develop linear angular correlation functions that relate the ^{29}Si NMR shift of the central silicon atom to the Si−O−Si angles surrounding it. The bonding nature of carbon atoms, whether 4-fold (sp^3) or 3-fold (sp^2) connected, impacts the chemical shift of $\{Si\}O_3C$ units and can be used to distinguish between Si−C bonding in the "glassy" SiCO host structure and at the interface to so-called "free" carbon. With the derived correlation functions, we analyze two representative experimental ^{29}Si NMR spectra and extract their angle distributions. Our results are in agreement with X-ray and neutron diffraction data. Probing for an interface between "free" carbon and "glassy" SiCO host in a C-rich SiCO material, we find no evidence of significant bonding between Si and three-connected (sp^2) C. Rather, the material exhibits a large fraction of wide Si−O−Si angles, which are typical of cage-like and zeolitic structures.

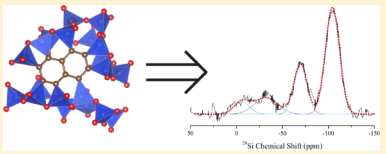

INTRODUCTION

Solid-state NMR is a powerful tool for structural analysis of disordered and complex materials.[1] The technique provides insight into the local chemical environment of nuclei and is complementary to structural information provided by diffraction and other spectroscopic methods (e.g., IR and Raman). Typically, interpretation of NMR spectra of amorphous materials is done by comparison with crystalline systems. However, disordered materials with a broad manifold of local environments, including unprecedented ones without well-defined crystalline analogues, pose a challenge for traditional analysis techniques and require new concepts to support structural characterizations.

In recent years, the gauge-including projector augmented wave method (GIPAW) and its combination with density functional theory (DFT-GIPAW) facilitates computation of NMR parameters in extended solids.[2] Successful prediction of chemical shifts and other NMR parameters was demonstrated for various crystalline and amorphous solids.[3−6] Combining NMR spectroscopy with GIPAW calculations of extended systems provides relevant information and supports structural characterization of complex solids.[7−11] For instance, NMR data of vitreous silica can be related to the Si−O−Si angle distribution and yields information about the appearance of small rings in the network structure.[3] An excellent review of progress and applications of GIPAW in various fields is given in the literature.[12]

Amorphous silicon oxycarbide (a-SiCO) ceramics are compounds of composition SiC_xO_y that are, typically, synthesized via thermal conversion of molecular or polymeric precursors into SiCO ceramics.[13] In recent years, these polymer-derived ceramics have been investigated and applied as structural and functional materials.[14−16] Notable features of a-SiCO are its disordered structure and resistance to crystallization: a-SiCO remains amorphous at temperatures where fused silica invariably crystallizes. Most SiCO ceramics obtained at 1000 °C display a stoichiometric oxycarbide glass, $SiC_xO_{(2-2x)}$, formally a mixture of SiO_2 and SiC, with additional "excess" carbon.[17] Annealing SiCO at 1450 °C ultimately yields SiC precipitates embedded in amorphous silica together with turbostratic or graphitic carbon. It is noteworthy that the quasi-binary SiO_2−SiC system contains no known crystalline compounds other than SiO_2 and SiC. Moreover, SiCO ceramics are only attainable through the molecular route, since the solubility of SiC in silica is less than 1%.[18−20]

Several studies applied NMR techniques to monitor conversions from molecular compounds to a-SiCO ceramics (e.g., from sol to gel to amorphous state), permitting insights into the structural evolution associated with these transitions.[21] After annealing at 1000 °C, ^{29}Si NMR spectra of amorphous SiCO feature several broad peaks, which are associated with local environments of "mixed" tetrahedra, $\{Si\}O_{4-n}C_n$. Since no crystalline SiCO structure with tetrahedra such as $\{Si\}O_3C$ or $\{Si\}O_2C_2$ exists, interpretation of ^{29}Si NMR spectra has been limited to quantification of the respective tetrahedra via integration of their peak area. The evolution of relative proportions of the peaks as a function of temperature can then be used to characterize phase separation in the amorphous state.[22] However, besides peak area no further structural information has been extracted from width, shape, or position of the peaks.

Received: October 3, 2014
Revised: November 26, 2014
Published: December 1, 2014

   dx.doi.org/10.1021/jp510021z | J. Phys. Chem. C 2014, 118, 29952−29961

There has been a long debate with respect to the nature of the "excess" carbon in a-SiCO. While Raman spectroscopy indicates that excess carbon is predominantly 3-fold (sp^2) coordinated and resembles graphene layers, the interface between such "graphitic carbon" and the surrounding SiCO host remains secluded. ^{13}C NMR spectroscopy of material obtained at 1000 °C shows two broad signals. One with large chemical shift anisotropy is attributed to 3-fold (sp^2) coordinated C, and the other signal with small anisotropy resembles the environment of C in SiC.[23] Several models have been proposed how the "free" carbon is embedded into the SiCO host matrix.[23,24] While most speculate about a "SiC-rich" interface between a silica-rich region and the free carbon, spectroscopic methods have provided no evidence of covalent bonding at the interface. Recent modeling studies indicated, however, that bonds between a graphitic segregation and Si atoms of the SiCO host matrix are energetically unfavorable.[25]

In this contribution we provide results of computational NMR spectroscopy of SiCO ceramics with the goal to enhance structural analysis of SiCO by experimental NMR spectroscopy. In the first section, we document the calibration of our approach using a set of models that has been used previously to analyze the structure of vitreous silica, a-SiO_2. Thereafter we analyze the dependency of the NMR signal of various $SiO_{4-n}C_n$-tetrahedra on the local structure, namely the Si−O−Si bond angles at that site. We will highlight the distinction between Si-sites bonded to 4-fold coordinated carbon (so-called sp^3-C) and Si-sites bonded to 3-fold coordinated (sp^2-C) carbon. Finally, we apply our computational results in the form of angular correlation functions to analyze experimental NMR data from the literature and "invert" their information to angle distribution functions. Additionally, we will model ^{29}Si NMR spectra and compare them with experimental data. On the basis of our analysis, we hypothesize on the nature of the connectivity between free carbon phase and host glass in SiCO ceramics.

METHODS

In the present study, we model a variety of silicon oxycarbide structures and compute ^{29}Si NMR shielding using the gauge including projector augmented wave (GIPAW) method[2] as implemented in the Quantum-ESPRESSO package.[26] Our approach follows the procedure previously outlined for amorphous silica[3] and uses the same set of 14 SiO_2 models (each containing 36 formula units of SiO_2) for the calibration of chemical shifts. We then generate 247 models of silicon oxycarbide, SiCO, displaying a variety of local environments for Si. Overall, more than 5000 Si sites and their corresponding chemical shifts are computed.

SiCO structures are generated using a modified Wooten−Winer−Weaire (WWW) algorithm.[25,27−30] Our models comprise glassy SiCO with "sp^3"-like C, which can be considered as a stoichiometric mixture of SiO_2 and SiC[30] as well as SiCO models with so-called "free" carbon embedded.[25] Experimentally, SiCO annealed at temperatures above 1000 °C contains "graphite-like" carbon[31,32] embedded in an amorphous glassy SiCO host matrix. Consequently, we model "free" carbon as aromatic units with "sp^2"-like C. Since a goal of our study is to find signatures of an interface between "free" carbon and the SiCO host matrix, we bond extended units of aromatic carbon (benzene, anthracene, one-dimensional strips) to Si atoms of the matrix. A detailed description of the network algorithm is given in ref 29.

Once model structures are obtained, we perform local optimizations including cell shape optimization using density functional theory as implemented in the Quantum-ESPRESSO code.[26] We use a kinetic energy cutoff of 80 Ry for the expansion of the wave function into a plane wave basis set and the Perdew−Burke−Ernzerhof (PBE)-generalized gradient approximation (GGA) method to approximate electron exchange and correlation.[33] The core electrons are described by norm-conserving Troullier−Martins pseudopotentials. For the GIPAW augmentation, we use two projectors in each angular momentum channel. The Brillouin zone is sampled at the Γ-point. Test calculations using a 2 × 2 × 2 k-point mesh showed no significant change in structural data or chemical shifts. Absolute chemical shifts are calculated using the GIPAW method and calibrated to α-quartz ($\delta_{iso} = -107.1$ from TMS[28]). This way, chemical shift values we present can be compared directly to experimental data.

RESULTS

SiO_4 Centers in a-SiO_2. The ^{29}Si isotropic chemical shift δ_{iso} in pure silica glass, a-SiO_2, is determined by the four Si−O−Si angles surrounding the Si nucleus (Figure 1a).[3,34−42]

Assuming that the four angles are not correlated and their contributions to δ_{iso} are independent, the chemical shift is given by

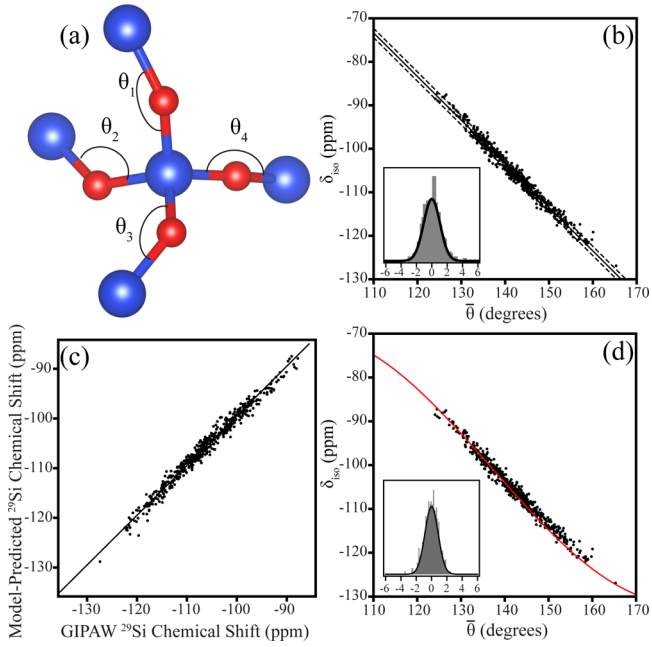

Figure 1. (a) A central silicon atom surrounded by four oxygen atoms indicating four different Si−O−Si angles. (b) Computed ^{29}Si chemical shift vs average of the adjacent Si−O−Si angles in a-SiO_2 fitted using eq 3, with $b = 36.9 \pm 1.0$ and $m = -1.00 \pm 0.01$. The inset shows a histogram of the δ_{iso} residuals fitted to a normal distribution with a standard deviation of 1.1 ppm. This deviation is also indicated as a dashed line bracketing the straight line of the fit to the data. (c) Comparison of the ^{29}Si chemical shifts predicted by the linear model vs values computed by GIPAW. (d) The same data used in (b) fitted with the trigonometric function, eq 2. Parameters are $k_1 = -108.1$, $k_2 = -13.7$, and $k_3 = -36.2$. The inset shows a histogram of the δ_{iso} residuals fitted to a normal distribution with standard deviation of 0.9 ppm.

dx.doi.org/10.1021/jp510021z | J. Phys. Chem. C 2014, 118, 29952−29961

$$\delta_{iso} = \frac{1}{4}\sum_{i=0}^{4} F(\theta_i) \quad (1)$$

with some angular correlation function $F(\theta)$ relating bond angle to chemical shift. A variety of functions $F(\theta)$ have been proposed based on experimental NMR spectra and crystal structure data.[3,34−42] A recent study investigating amorphous SiO_2 used a trigonometric expansion for $F(\theta)$

$$F(\theta) = k_1 + k_2\cos(\theta) + k_3\cos(2\theta) \quad (2)$$

with three parameters fitted to the data.[3] However, we found these parameters to be strongly correlated, with a small change in the data set causing large changes in k_1, k_2, and k_3. Thus, we propose to use a simple linear correlation function[37,38,40,42]

$$F(\theta) = m\theta + b \quad (3)$$

or

$$\delta_{iso} = m\bar{\theta} + b \quad (4)$$

with only two parameters to be fitted to the data. The linear relation implies that the average value of the four Si−O−Si angles surrounding the Si nucleus relates directly to the chemical shift. Moreover, the simple forms of eqs 3 and 4 facilitate the inversion from experimental data of chemical shifts to an angle distribution function for the angle θ later on.

Our results of the set of 14 SiO_2 models, the same set of models previously computed by Charpentier et al.[3] are shown in Figure 1b. Each model comprises 36 formula units SiO_2. The 504 SiO_4 environments are plotted in Figure 1b. The linear fit yields $m = -1.00 \pm 0.01$ and $b = 36.9 \pm 1.0$. The inset shows a histogram of the residue, displaying the difference between computed chemical shift and predicted shift using the angular correlation function. The residuals are distributed normally with a standard deviation of 1.1 ppm. A direct comparison is also shown in Figure 1c, where we plot the predictions of the linear model versus the GIPAW-computed chemical shift values directly.

Figure 1d uses the same ^{29}Si isotropic chemical shifts for 504 SiO_4 centers as Figure 1b, but fitted with the trigonometric expansion used by Charpentier et al.[3] of eq 2. We obtain $k_1 = -108.1$, $k_2 = -13.7$, and $k_3 = -36.2$. The histogram of the residues inserted in Figure 1d yields $\sigma = 0.9$ ppm, only a marginable improvement in comparison to the linear fit. The more complex trigonometric expansion fits the data slightly better, but with the cost of an additional parameter and a more complex functional form. Moreover, a comparison of fit parameters k_1, k_2, and k_3 obtained here with those presented previously by Charpentier et al.[3] [$k_1 = -102.36$, $k_2 = -6.95$, and $k_3 = -33.82$] shows a strong variation of the parameters. Indeed, parameters k_1, k_2, and k_3 are correlated and change significantly, if data are added or omitted from the set. Consequently, we regard the simplicity of the linear angular correlation function being justified by (i) a comparable residual, (ii) the use of one fewer parameter, and—anticipating later results—(iii) by the simplicity of the transformation relating NMR data to an angle distribution.

A linear fit has previously been applied to relate the averaged B−O−B angle around a B nucleus to the chemical shift of ^{11}B in boria, B_2O_3.[43] Comparing different approaches used before,[41,44,45] the authors[43] indicated that for the region of interest the trigonometric expansion (eq 2) yields approximately a linear dependence anyway. The same argument holds true for the data we show for a-SiO_2.

Structural Inversion in SiO_2. Using the linear angular correlation function, the inversion of experimental NMR spectra is given by

$$\bar{\theta} = (\sigma_{iso} - b)m^{-1} \quad (5)$$

By virtue of the simple linear function, a Gaussian distribution of ^{29}Si NMR data is easily transformed back into a Gaussian distributed angle distribution function. Assuming that all N angles contributing to the chemical shift are independent, the widths of NMR data and angle distribution are related, $\sigma_\theta = \sqrt{N} \times \sigma_\delta$ [ppm/deg]. If non-Gaussian distributions are assumed, a kernel transformation can be used (eqs 9 and 10 of Charpentier[3]), or the angle distribution can be found using a Monte Carlo procedure.

We apply our model of structural inversion to the experimental ^{29}Si NMR data published by Clark.[46] The experimental data are well described by a Gaussian function centered at −111.2 ppm with a full width at half-maximum (fwhm) of 12 ppm (Figure 2a). Structural inversion using the linear angular correlation function yields an angle distribution (Gaussian) centered at 147.7° with $\sigma = 10.2°$. This is very close to previous results published by Charpentier,[3] 148.4 (σ = 10.8)°, which is not surprising given that we use the same set of models. It also corresponds well to results[46] obtained by neutron diffraction, 146.7 ± 7.3°. A second sample from the literature is by Mahler and Sebald.[47] The chemical shift signal can be adequately described with a Gaussian centered at −111.8 ppm with a fwhm of 9.4 ppm. When inverted with our linear function, this spectrum yields an angle distribution centered at $\bar{\theta}$ = 148.3 (σ = 8.1)°. Once again, this nicely agrees with experimental results based on a combined neutron and X-ray diffraction study of Neuefeind and Liss,[48] who report $\bar{\theta}$ = 148.3 (σ = 7.5)° (Figure 2b).

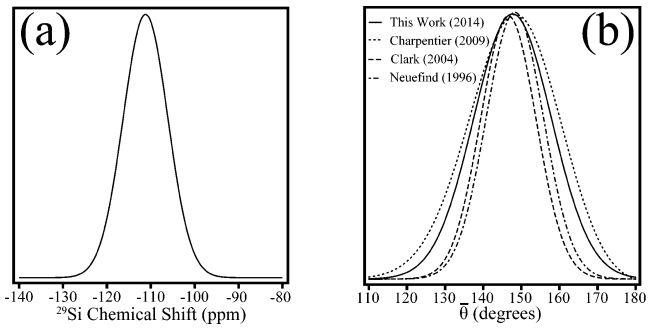

Figure 2. (a) Experimental NMR spectra of amorphous silica analyzed by Clark.[46] (b) Results of various inversion techniques on vitreous silica.

We confirmed the correspondence between extracted angle distribution and experimental NMR data with Monte Carlo simulations. Four angles are drawn randomly from the distribution, and the angular correlation function is applied to yield a chemical shift. We find that a normal distribution for angles is sufficient to yield the correct distribution for the chemical shift data. Moreover, the difference between using our linear correlation function and the more sophisticated version by of Charpentier et al.[3] is insignificant within the errors of the fit.

dx.doi.org/10.1021/jp510021z | J. Phys. Chem. C 2014, 118, 29952−29961

^{29}Si NMR of SiCO Ceramics. Experimental ^{29}Si NMR data for SiCO ceramics typically shows four different peaks of δ_{iso}. An example is shown in Figure 8. The peaks are attributed to Si nuclei within $\{Si\}O_4$, $\{Si\}O_3C$, $\{Si\}O_2C_2$, and a combination of $\{Si\}OC_3$ and $\{Si\}C_4$ tetrahedra, with peak maxima typically located near −108, −70, −25, and −5 ppm, respectively.[49−52] A structural analysis based on the NMR data will require quantitative means to distinguish between bonding of Si to tetrahedral carbon (carbidic, or sp^3) and bonding of Si to planar coordinated carbon (aromatic or graphitic, sp^2). Bonding of Si to sp^3-C will occur in glassy (transparent) SiCO, which can be regarded as a mixture of SiO_2 and SiC.[17,25,30,53] While the solubility of SiC in silica is negligible, polymer routes offer pathways to glassy SiCO with a composition of up to 33 mol % SiC.[22] On the other hand, bonding of Si to sp^2-C will occur in a preceramic state, if for instance aromatic side groups (e.g., phenyl) have been used during synthesis.[51] Bonding of Si to sp^2-C carbon after producing the ceramic (e.g., heat treatment at 1200 °C) may indicate covalent bonds at the interface between the glassy SiCO host matrix and carbon segregations (so-called "free carbon"). Experimentally, a distinction between bonding of Si to sp^3-C or sp^2-C in the polymeric state is indicated by a shift of the NMR signal by 5−10 ppm.[32] Bonding of Si to one aliphatic group (and three oxygen atoms, Figure 3a) is manifested in chemical shifts around −70 to −74 ppm, while Si bonded to a vinyl or aromatic group results (Figure 3b) in chemical shifts located at −78 to −81 ppm.

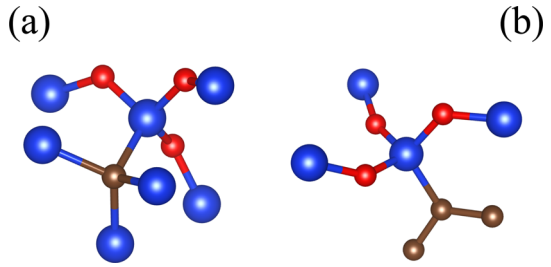

Figure 3. Two environments of $\{Si\}O_3C$ tetrahedra considered. (a) Silicon bonded to sp^3-C as in glassy SiCO. (b) Silicon atom bonded to sp^2-C modeling the interface between SiCO glass and free carbon.

We generated a variety of models reflecting the different Si−C bonding situations outlined above. Modeling glassy SiCO followed procedures we described before.[22,25] In these models, all C atoms remained 4-fold connected to Si. Models with carbon segregations were constructed by inserting structure fragments (e.g., C_6-ring, fused C_6-rings; 1-D strips of C) into silica models. Segregations are connected to the host matrix via Si−C bonds. All models with segregations comprise solely 3-fold coordinated C (sp^2-C), which bonds either to other C, to Si, or to H. We subjected the models to our bond switching algorithm, a procedure that optimizes the network topology including interfacial bonding.[25,29] The obtained network structures were optimized and computed using the described DFT methods. Si atoms in every model were analyzed according to their local environment. We first discuss the ^{29}Si NMR chemical shifts in structures comprising only sp^3-C, followed by local environments of Si in systems comprising sp^2-C.

$\{Si\}O_4$ Centers in Glassy SiCO Models. In analogy to our analysis of the isotropic chemical shift in a-SiO_2, we collected data from $\{Si\}O_4$ centers in glassy SiCO models. A total of 2940 centers contribute to the analysis. Assuming the linear relation of eq 3 as before, a fit to the data yields b = 33.4 ± 0.5 and m = −0.976 ± 0.004 (Figure 4a). A comparison between

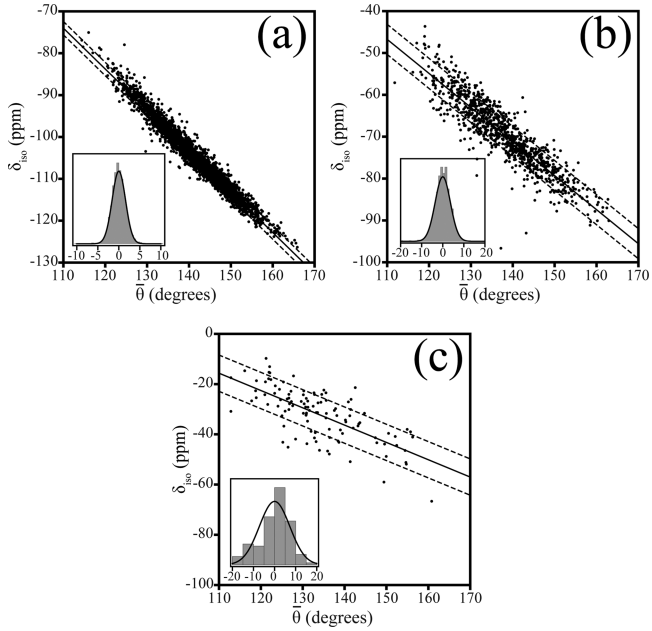

Figure 4. Computed ^{29}Si chemical shift vs average Si−O−Si angles surrounding the Si nucleus in SiCO models without free carbon. The solid lines are linear fits to each set of data, using eq 3. The insets show histograms of the δ_{iso} residuals fit with a normal distribution with a standard deviation. This deviation is also indicated as dashed lines bracketing the linear fits to the data. (a) $\{Si\}O_4$ centers with parameters b = 33.4 ± 0.5 and m = −0.976 ± 0.004 and residual standard deviation of 1.6 ppm. (b) $\{Si\}O_3C$ centers with parameters b = 42.8 ± 1.8 and m = −0.81 ± 0.01 and residual standard deviation of 3.6 ppm. (c) $\{Si\}O_2C_2$ centers with parameters b = 60.2 ± 8.5 and m = −0.69 ± 0.06 and residual standard deviation of 7.2 ppm.

computed (GIPAW) and predicted δ_{iso} is included in the inset of Figure 4a as residual (deviation of computed from predicted value) distribution. It shows a standard deviation of 1.6 ppm. Using a trigonometric expansion as in eq 2 results in a residual with an only marginally smaller σ of 1.4 ppm.

$\{Si\}O_3C$ Centers in Glassy SiCO Models. The glassy SiCO models provide a total of 933 $\{Si\}O_3C$ centers, where C is 4-fold (sp^3) connected to Si. The computed chemical shift data are, surprisingly, well described by the average of angles at the three surrounding oxygen only. The correlation is shown in Figure 4b. The data are fitted with a linear function according to eq 3, with slope (m) = −0. 81 ± 0.01 and intercept b = 42.8 ± 1.8. The residual, included in Figure 4b as inset, shows a standard deviation of 3.6 ppm.

We made efforts to improve the modeling of chemical shifts of $\{Si\}O_3C$ centers by involving the Si−C bond and its geometrical parameters. Some of our attempts are shown in Figure 5. However, neither the Si−C bond length itself nor its deviation from an ideal value (e.g., 188 pm) impacts the computed chemical shift in a systematic way. This is best demonstrated by a residual, the difference between computed chemical shift and the value predicted by the angular correlation function involving only the three surrounding angles at O. This graph is included in Figure 5c. To study this further, we performed comparative calculations of chemical shifts of some molecular compounds (e.g., $Si(OH)_3CH_3$).

dx.doi.org/10.1021/jp510021z | J. Phys. Chem. C 2014, 118, 29952−29961

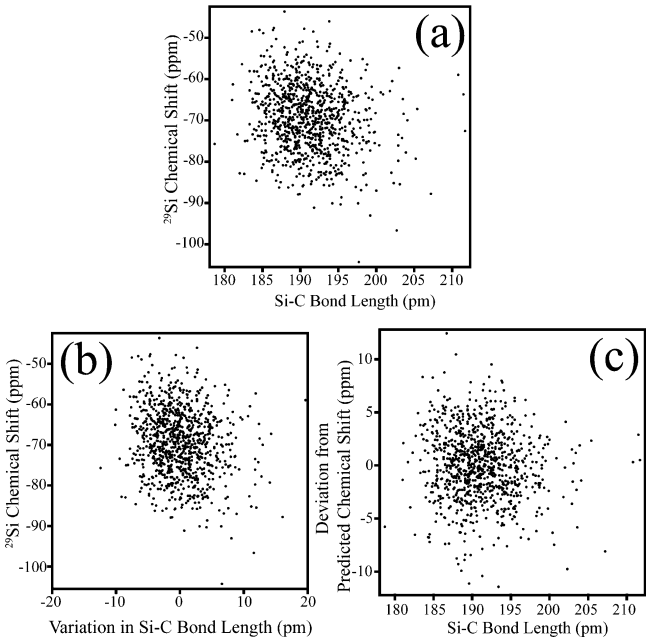

Figure 5. Analysis of GIPAW chemical shifts and Si−C bond length at $\{Si\}O_3C$ centers. Plots show (a) GIPAW chemical shift vs Si−C bond length, (b) GIPAW chemical shift vs deviation from average Si−C bond length, and (c) residual vs Si−C bond length.

These show a dependency of the chemical shift on the Si−C bond length, if the surrounding bond angles are kept fixed. However, the dependency is only small ($\Delta\delta_{iso}$ = 0.24 ppm × Δl/pm, with Δl being the bond length variation). In the extended systems the effect, if present, is not strong enough to substantiate a correlation.

$\{Si\}O_2C_2$ Centers in Glassy SiCO Models. The glassy SiCO models also contain 110 $\{Si\}O_2C_2$ centers, for which we plot the computed chemical shift as a function of the average over the (only) two angles at surrounding O atoms (Figure 4c). A linear fit yields the parameters m = −0.69 ± 0.06 for the slope and b = 60.2 ± 8.5 for the y-intercept. Once again we tested for possible dependency of the chemical shift on geometrical parameters involving the Si−C bond but did not find a systematic correlation. Hence, if such a dependency exists, its impact is significantly smaller than the impact of the angles at surrounding O atoms. The residual of the fit is significantly broader than before, with a standard deviation of 7.2.

Centers in Structures Containing "Free" (Graphitic) Carbon. The so-called "free" carbon phase is an essential constituent of many SiCO ceramics. Its genesis depends strongly on processing conditions, including the structure of precursors and the temperature to which the ceramic was annealed.[22,31,51,54−56] It is an accepted viewpoint that after annealing at temperatures at and above 1000 °C the "free" carbon phase has segregated into graphite-like carbon units surrounded by a glassy SiCO matrix. A persisting and unresolved question is the presence and nature of an interface between the "free" carbon phase and the SiCO host glass matrix in the material obtained at 1000 °C and above. One proposed scenario involves a C-rich SiCO phase bonding via Si−C bonds to the graphitic phase.[24,57] Modeling studies, on the other hand, have indicated a significant energy penalty of such an interface and proposed that the "free" carbon phase will tend to debond completely from the surrounding SiCO glass matrix.[25] Residual H in the material may even facilitating this change. The appearance of Si−C bonds, with Si bonded to sp^2-C, may be a test for the likelihood of these scenarios.

Thus, we set out and created models of glassy SiCO and silica containing graphitic segregations in the form of small aromatic units or extended one-dimensional strips of graphene. We bonded these units via Si−C bonds to the glass network structure and, applying the network algorithm, optimized network topology, including the interface between host and segregation. Thereafter, we applied the standard DFT procedure outlined above and computed ^{29}Si NMR data. The SiCO models with "free" carbon comprise $\{Si\}O_4$ and $\{Si\}O_3C$ centers only. Some representative models are shown in Figure 6.

$\{Si\}O_4$ Centers in SiCO Models with "Free" Carbon. Similar to our analysis of the isotropic chemical shift in a-SiO_2 and in glassy SiCO, we collected data from $\{Si\}O_4$ centers in SiCO models comprising "free" carbon. A total of 4647 centers contribute to our analysis shown in Figure 7a. Plotting the average of the four Si−O−Si angles versus the ^{29}Si NMR shift for the $\{Si\}O_4$ centers, we obtain a slope (m) of −1.001 ± 0.003 and a y-intercept (b) of 36.9 ± 0.4. Once again we include the residual (standard deviation of 1.5 ppm) in Figure 7a.

$\{Si\}O_3C$ Centers in SiCO Models with "Free" Carbon. The SiCO models with "free" carbon comprise 828 $\{Si\}O_3C$

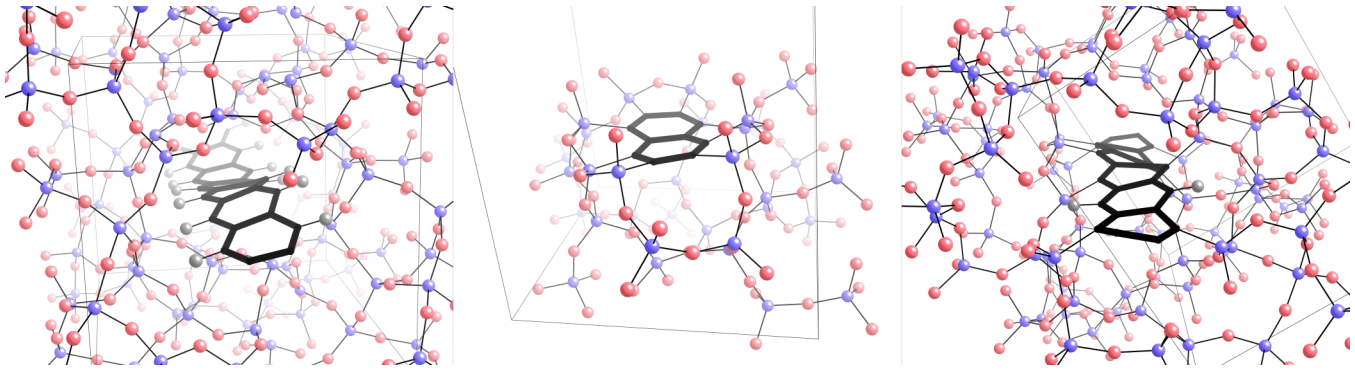

Figure 6. Representative structural models of "free" carbon based on fused benzene rings with various patterns of embedding into the host glass: (left) polycene embedded but not connected to the host glass, (middle) naphthalene "fully" connected via eight Si−C bonds, and (right) a polycene partially connected, with some remaining C−H bonds.

dx.doi.org/10.1021/jp510021z | J. Phys. Chem. C 2014, 118, 29952−29961

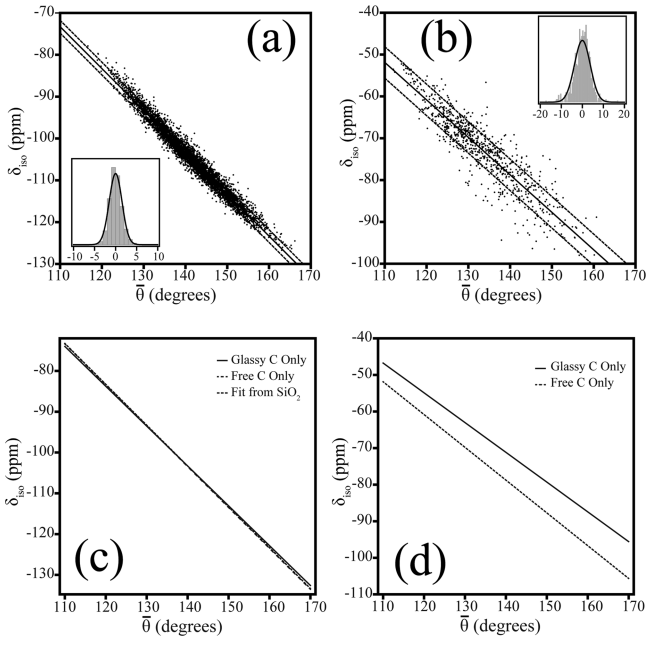

Figure 7. (top) Computed ^{29}Si chemical shift vs average Si−O−Si angles surrounding the Si nuclei in SiCO models containing free carbon. The solid lines are linear fits to the data, using eq 3. The inset shows a histogram of the δ_{iso} residuals, fit with a normal distribution. The standard deviation of the residual is also indicated as dashed lines bracketing the linear fit to the data. (a) $\{Si\}O_4$ centers with parameters with b = 36.9 ± 0.4 and m = −1.001 ± 0.003 and residual standard deviation of 1.5 ppm. (b) $\{Si\}O_3C$ centers with parameters b = 46.7 ± 2.0 and m = −0.90 ± 0.01 and residual standard deviation of 3.8 ppm. The difference to Figure 4b is that Si bonds to C(sp^2) rather than C(sp^3). (bottom) Comparison for the fits of centers in models containing only glassy carbon vs the fit for models containing free carbon: (c) $\{Si\}O_4$ centers; (d) $\{Si\}O_3C$ centers (comparing fits of Figures 4b and 5b).

centers, with Si bonding to 3-fold coordinated (sp^2) C. As before, we use the average of the three angles at the surrounding O only to model the computed chemical shift data. Approaches to include the Si−C bond length did not provide systematic improvements. The data shown in Figure 7b are fitted with a linear function with slope (m) = −0.90 ± 0.01 and intercept b = 46.7 ± 2.0. The residual shows a standard deviation of 3.8 ppm.

Comparison of NMR Calculations between the Two Populations. We compare the three (slightly) different angular correlation functions for $\{Si\}O_4$ centers in models of SiO_2, glassy SiCO, and SiCO containing "free" carbon in Figure 7c. The largest deviation between the fits is smaller than 1 ppm and occurs only at extreme angles, 110° or 170°. Within the expected range of most Si−O−Si angles, approximately 120°−160°, all three populations are described equally well by the same fit, not at least since the residual of each fit is 1 ppm or larger. The data of $\{Si\}O_4$ centers in SiCO, from models with sp^3-C and sp^2-C, may even be combined (total of 5880 centers) to yield a correlation function with m = −0.976 ± 0.003 and b = 33.4 ± 0.4 and a residual with width of 1.6 ppm.

The situation is quite different for SiO_3C centers occurring in SiCO, however. A comparison is plotted in Figure 7d and shows the significant difference between bonding of Si to sp^3-C or bonding of Si to sp^2-C. For angles between 130° and 160° the two correlation functions yield a difference of 5−10 ppm in the NMR signal. Thus, our result reflects trends observed in experimental NMR studies, which reported a downfield shift of the ^{29}Si NMR signal in organosilyl compounds upon replacement of methyl groups with phenyl groups.[58,59] A similar trend was reported to occur in SiCO ceramics,[31] where the observed broad ^{29}Si NMR signal centered at −81 ppm (Si connected to phenyl) or −78 ppm (bonding to vinyl groups) shifts during the polymer-to-ceramics conversion into a range from −70 to −74 ppm reflecting the incorporation of Si−C bonds (sp^3-C) into the structure. Here we provide a quantitative description of these changes, which will allow us to analyze bonding environments at the interface between the glass and the free carbon. The significant difference between bonding Si to sp^3-C and bonding Si to sp^2-C will allow us to analyze the $\{Si\}O_3C$ peaks of experimental spectra and to differentiate between Si−C bonds in the glassy phase and Si−C of interfacial bonding between SiCO glass and free carbon.

Structural Inversion of Experimental SiCO NMR Spectrum. The angular correlations for various Si sites in SiCO ceramics facilitate the extraction of information about the angle distribution at O atoms from experimental NMR spectra. Thus, we follow a similar protocol as applied previously to SiO_2.[3] Structural inversion in SiCO, however, provides more than just the angle distribution at O, since more data than just a $\{Si\}O_4$ peak is available. As pointed out before, we may gain insight into the existence and prominence of the interface between SiCO glass and "free" carbon. A technical procedure to analyze ^{29}Si NMR data of SiCO may start with an analysis of the $\{Si\}O_4$ peak, from which the angle distribution at O is deduced. Assuming a homogeneous distribution of all Si−O−Si linkages in the material, this angle distribution can be used to model the $\{Si\}O_3C$ peak, either for sp^3-C or sp^2-C. A comparison with experimental spectra may then yield quantitative information about Si−C bonding to sp^3-C or sp^2-C and, as a consequence, the amount of Si atoms participating in an interface toward a "free" carbon phase. Conversely, angle information from all NMR peaks may be collected and checked for consistency. In the following, we will apply this method for two selected SiCO materials: one with a low "free" carbon content, resembling a glassy SiCO,[22] and another C-rich sample of SiCO with high amount of "free" C.[51]

Structural Inversion of SiCO NMR Data: Low "Free" Carbon Content. In a recent paper, Brequel et al.[22] reported experimental NMR data of a SiCO material with low "free" carbon content annealed at 1000 °C. The composition of the material is $SiC_{0.27}O_{1.49}$, which resembles a phase composition of 0.255SiC + 0.745SiO_2 + 0.015C_{free}. An average angle of 140.6° at O was deduced from neutron diffraction studies. We reproduce the experimental ^{29}Si NMR spectrum in Figure 8 together with a decomposition of the individual peaks using Gaussian functions.

The $\{Si\}O_4$ peak can be fitted with a single Gaussian function centered at −104.5 ppm with a fwhm of 18.1. Using this data together with the angular correlation function for SiO_4 centers [combined fit with m = −0.976 and b = 33.4], we obtain an angle distribution centered at 141.2° with a standard deviation of σ = 15.3°. This compares with the results of neutron diffraction (140.6°), which included, however, no width. Hence, NMR data and neutron diffraction data show consistent results.

The $\{Si\}O_3C$ peak of the spectrum is readily fitted using a single Gaussian function centered at −69.7 ppm with a fwhm of 16.8. Using two Gaussian functions to fit the data yields two curves centered at −69.1 ppm, but with different widths (fwhm

dx.doi.org/10.1021/jp510021z | J. Phys. Chem. C 2014, 118, 29952−29961

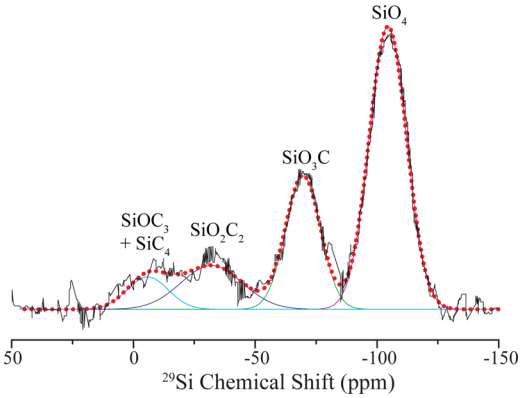

Figure 8. Experimental ^{29}Si NMR spectrum of SiCO from ref 22 (sample $T^{H}D^{H}2$ pyrolyzed at 1000 °C). We include a fit using Gaussian functions of the individual peaks for $\{Si\}O_4$, $\{Si\}O_3C$, and $\{Si\}O_2C_2$ environments and a fourth Gaussian fitting the combined $\{Si\}OC_3-\{Si\}C_4$ peak. The combination of the four fit functions yields the red dotted line superimposed on the spectrum.

of 13.2 and 39.2) and a relative proportion of 3:1 by area. However, the quality of the fit does not improve significantly, and consequently, we continue our analysis using the single Gaussian fit only. Inverting this fit to structural data using the correlation function $\{Si\}O_3C$ in glassy SiCO (sp^3-C) yields an angle distribution centered at 138.3° (σ = 16.0°). If we were to use the data together with the angular correlation functions for $\{Si\}O_3C$ centers of Si bonded to sp^2-C, we would receive a distribution of angles with a maximum at 130.0° (σ = 16.0°). Thus, assuming that Si bonds to sp^3-C only provides an angle distribution consistent with the $\{Si\}O_4$-peak data, supporting in turn the concept of a homogeneous SiCO glass. Additional support comes from the $\{Si\}O_2C_2$ peak data, which are best fitted by a Gaussian function centered at −32.1 ppm with a fwhm of 22.0. Inverting this peak yields an angle distribution with maximum at 135.5° and width σ = 18.3°.

Comparing the location of the three maxima of angle distributions at O that we obtain from inversion of $\{Si\}O_4$, $\{Si\}O_3C$, and $\{Si\}O_2C_2$ NMR peaks, 141.2°, 138.3°, and 135.5°, we find that these are consistent with the neutron data (140.6°), assuming a weighted average. The shift of the position of the maximum from 141.2° down to 135.5° may reflect increasing strain within the various rings of the network structure, some containing only Si and O atoms and some incorporating C. In a random network structure of SiCO glass rings of different sizes and different atom participation occur.[30] A Si atom with four surrounding O atoms, a $\{Si\}O_4$ center is not necessarily located within a ring containing a C (but it may). On the other hand, $\{Si\}O_3C$ centers certainly are, and $\{Si\}O_2C_2$ centers are member of at least one ring containing at least two C atoms. Rings involving C atoms are typically smaller (lower member count) and smaller ring sizes comprise smaller bond angles at O atoms.[3] Hence, the trend from $\{Si\}O_4$ to $\{Si\}O_3C$ and $\{Si\}O_2C_2$ centers appears to be consistent with a network model of glassy SiCO. Therefore, our model is aligned with previous experimental and computational findings in describing the structure of SiCO and provides a simple way to extract this information from NMR spectra.

Structural Inversion of SiCO NMR Data: High "Free" Carbon Content. ^{29}Si NMR data of a SiCO material with high "free" carbon content [$0.495SiC + 0.505SiO_2 + 1.095C_{free}$] is taken from the works of Radovanovic.[51] A reproduction of the experimental data is shown in Figure 9 together with a fit to the data using Gaussian functions. A major difference to the data of

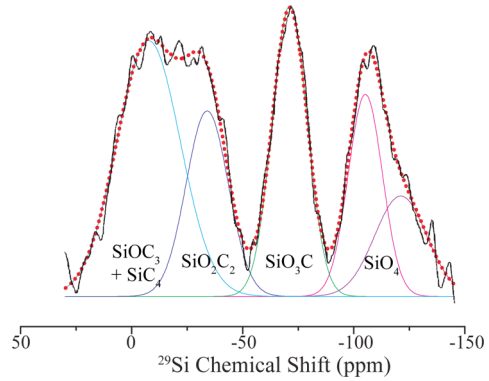

Figure 9. Experimental ^{29}Si NMR spectrum of the P1 sample from Radovanovic.[51] We include a fit to the data using Gaussian functions of the individual peaks for $\{Si\}O_4$ (two peaks), $\{Si\}O_3C$, and $\{Si\}O_2C_2$ environments and one Gaussian for the combined $\{Si\}OC_3-\{Si\}C_4$ peak. The combination of the individual curves yields the red dotted line superimposed on the spectrum.

Brequel et al.[22] (Figure 8) is the extended peak for SiO_4 centers, which shows a significant skewness. It is best fitted by two Gaussians: a first centered at −105.2 ppm with a fwhm of 18.1 ppm and a second at −121.2 with a fwhm of 27.6 ppm [relative proportion 3:2 by area]. Inversion of the first SiO_4 peak (at −105.2 ppm) yields an angle distribution at O with an average angle of 142.0° and standard deviation σ = 15.4°. The second peak yields an average angle of 158.4° with σ = 23.4°. Based on its position, width, and from the absence of other likewise peaks, it can be followed that this signal originates from the SiCO structure and is not a spinning sideband. Hence, this sample of C-rich SiCO contains two different populations of Si−O−Si angles. A first one is similar to that in "typical" SiCO, while the second one reflects significantly larger bond angles—which may be a special feature of this SiCO with high "free" C content.

We can fit the $\{Si\}O_3C$ peak with a single Gaussian centered at −71.2 ppm with fwhm = 18.5 ppm. Using two Gaussians yields maxima at −73.1 and −63.0 ppm, with fwhm of 15.0 and 11.3, respectively, and a ratio of peak areas of 3:1. However, the quality of the fit does not improve significantly. Moreover, an expected population of Si−C (sp^2-C) bonds would yield a signal shifted downward from the main peak, not upward. Consequently, we use the data of the single Gaussian only. Inverting this data—using the correlation function for glassy SiCO—we find an angle distribution centered at 140.0° with σ = 15.8°. Finally, the $\{Si\}O_2C_2$ peak centered at −34.0 ppm with fwhm = 22.4 ppm yields an angle distribution centered at 136.7° with σ = 19.0°.

Collecting the data of our analysis, we find that $\{Si\}O_4$ peak (only the first), $\{Si\}O_3C$ peak, and $\{Si\}O_2C_2$ peak together indicate a homogeneous SiCO glass, just as found for the glassy SiCO by Brequel et al. that we analyzed above. The shift in the maximum of the angle distribution at O atoms (from 142.0° over 140.0° to 136.7°) once again indicates increasing ring strain in rings containing more and more C atoms. Suspiciously absent is, however, a signal for the bonding of Si to sp^2-C—expected to be present in a material, which contains a large amount of "free" carbon. The fitting of the NMR data does not show a second peak with significant proportion in the expected

dx.doi.org/10.1021/jp510021z | J. Phys. Chem. C 2014, 118, 29952−29961

range. If the peak centered at −71.2 ppm would be, at least in parts, generated by $\{Si\}O_3C$ centers with Si bonding to sp^2-C, the angle distribution at the surrounding O atoms would show a maximum at 131.5°. However, neither the $\{Si\}O_4$ peak nor the $\{Si\}O_2C_2$ peak indicates significant contributions from such a Si−O−Si bond population. Hence, we conclude that this sample does not contain significant bonding between Si and sp^2-C. Consequently, we do not find a covalently bonded interface between graphitic segregations and the SiCO host.

The second $\{Si\}O_4$ peak may yield indirect support for this conclusion. As stated, it reflects another population of Si−O−Si angles centered at 158.4°. Such large angles are found at channels, cages, and voids in some zeolite minerals, for example mordenite,[60] with angles of 170°, stilbite[61] (157° and 173°), and heulandite[58] (162°). It is very likely that this SiCO with a high amount of "free" C also contains large channels, cages, and voids and that the Si−O−Si angle population reflects a large proportion of internal surfaces surrounding such open space. It may well be that this open space is filled with "free" carbon. Indeed, small-angle X-ray scattering of SiCO ceramics containing "free" carbon showed contrast variation at the nanometer length scale, which is indicative of a domain structure of this material.[24,62] The domain structure of SiCO ceramics containing free carbon has subsequently found significant resonance in the scientific community, and different concepts about structural models of SiCO have been developed.[23−25,32] Our analysis presented here supports the idea that segregation of "free" carbon forces the formation of zeolite-like features during the genesis of the SiCO material. This echoes the model proposed by Widgeon et al.,[23] which has nanometer-scale "mass-fractal" voids filled with graphitic free carbon. However, we see no evidence for a C-rich SiCO interface adjacent to these voids.

CONCLUSION

Using modeling of extended structures together with electronic structure calculation, including the GIPAW method, we relate structural features of an amorphous SiCO ceramic to its ^{29}Si NMR chemical shift spectrum. Our method extracts the Si−O−Si angle distributions of mixed tetrahedral environments, $\{Si\}O_4$, $\{Si\}O_3$, and $\{Si\}O_2C_2$ and, furthermore, the connectivity of C bonded to Si in $\{Si\}O_3C$ units.

Inverting experimental data, we receive Si−O−Si angle distributions that agree with available neutron data. In particular, Si−O−Si angles in rings comprising C atoms are, on average, smaller than in rings without C atoms. Furthermore, analysis of some C-rich SiCO compound shows no significant amount of Si atoms bonding to three-connected C atoms. Rather surprisingly, the material exhibits a significant proportion of wide Si−O−Si angles, which are typical of internal surfaces in cage-like structures and zeolites. The method presented in this work provides a tool to enhance experimental capabilities to use ^{29}Si NMR data for the analysis of complex materials.

AUTHOR INFORMATION

Corresponding Author

*E-mail pkroll@uta.edu (P.K.).

Notes

The authors declare no competing financial interest.

ACKNOWLEDGMENTS

This work was supported by the NSF (DMR-0907117) and by the US AFOSR (Dr. Ali Sayir) and NASA (Dr. Anthony Calomino) under the National Hypersonic Science Center for Materials and Structures (AFOSR contract no. FA9550-09-1-0477). The authors are indebted to Gian-Domenico Soraru, Ralf Riedel, Florence Babonneau, Christel Gervais, and Scarlett Widgeon for useful discussions. Computational work was made possible through generous grants by the Texas Advance Computing Center in Austin, TACC, Texas.

REFERENCES

(1) Eckert, H.; Ribeiro, S. L.; Santagneli, S.; Nalin, M.; Poirier, G.; Messaddeq, Y. Glasses on the Nanoscale. In *Springer Handbook of Nanomaterials*; Vajtai, R., Ed.; Springer: Berlin, 2013; pp 665−692.

(2) Pickard, C. J.; Mauri, F. All-Electron Magnetic Response with Pseudopotentials: NMR Chemical Shifts. *Phys. Rev. B* **2001**, *63*, 245101.

(3) Charpentier, T.; Kroll, P.; Mauri, F. First-Principles Nuclear Magnetic Resonance Structural Analysis of Vitreous Silica. *J. Phys. Chem. C* **2009**, *113*, 7917−7929.

(4) Ferlat, G.; Charpentier, T.; Seitsonen, A. P.; Takada, A.; Lazzeri, M.; Cormier, L.; Calas, G.; Mauri, F. Boroxol Rings in Liquid and Vitreous B_2O_3 from First Principles. *Phys. Rev. Lett.* **2008**, *101*, 065504.

(5) Pedone, A.; Charpentier, T.; Menziani, M. C. The Structure of Fluoride-Containing Bioactive Glasses: New Insights from First-Principles Calculations and Solid State NMR Spectroscopy. *J. Mater. Chem.* **2012**, *22*, 12599−12608.

(6) Profeta, M.; Mauri, F.; Pickard, C. J. Accurate First Principles Prediction of ^{17}O NMR Parameters in SiO_2: Assignment of the Zeolite Ferrierite Spectrum. *J. Am. Chem. Soc.* **2002**, *125*, 541−548.

(7) Hanna, J. V.; Smith, M. E. Recent Technique Developments and Applications of Solid State NMR in Characterising Inorganic Materials. *Solid State Nucl. Magn. Reson.* **2010**, *38*, 1−18.

(8) Charpentier, T.; Menziani, M. C.; Pedone, A. Computational Simulations of Solid State NMR Spectra: A New Era in Structure Determination of Oxide Glasses. *RSC Adv.* **2013**, *3*, 10550−10578.

(9) Ashbrook, S. E.; Dawson, D. M. Exploiting Periodic First-Principles Calculations in NMR Spectroscopy of Disordered Solids. *Acc. Chem. Res.* **2013**, *46*, 1964−1974.

(10) Pallier, C.; Leyssale, J.-M.; Truflandier, L. A.; Bui, A. T.; Weisbecker, P.; Gervais, C.; Fischer, H. E.; Sirotti, F.; Teyssandier, F.; Chollon, G. Structure of an Amorphous Boron Carbide Film: An Experimental and Computational Approach. *Chem. Mater.* **2013**, *25*, 2618−2629.

(11) Pedone, A.; Gambuzzi, E.; Menziani, M. C. Unambiguous Description of the Oxygen Environment in Multicomponent Aluminosilicate Glasses from ^{17}O Solid State NMR Computational Spectroscopy. *J. Phys. Chem. C* **2012**, *116*, 14599−14609.

(12) Bonhomme, C.; et al. First-Principles Calculation of NMR Parameters Using the Gauge Including Projector Augmented Wave Method: A Chemist's Point of View. *Chem. Rev.* **2012**, *112*, 5733−5779.

(13) Colombo, P. *Polymer Derived Ceramics: From Nano-Structure to Applications*; DEStech Publications, Inc.: Lancaster, PA, 2010.

(14) Meier, A.; Weinberger, M.; Pinkert, K.; Oschatz, M.; Paasch, S.; Giebeler, L.; Althues, H.; Brunner, E.; Eckert, J.; Kaskel, S. Silicon Oxycarbide-Derived Carbons from a Polyphenylsilsequioxane Precursor for Supercapacitor Applications. *Microporous Mesoporous Mater.* **2014**, *188*, 140−148.

(15) Konno, H.; Kasashima, T.; Azumi, K. Application of Si−C−O Glass-Like Compounds as Negative Electrode Materials for Lithium Hybrid Capacitors. *J. Power Sources* **2009**, *191*, 623−627.

(16) Zhuo, R.; Colombo, P.; Pantano, C.; Vogler, E. A. Silicon Oxycarbide Glasses for Blood-Contact Applications. *Acta Biomater.* **2005**, *1*, 583−589.

(17) Corriu, R. J. P.; Leclercq, D.; Mutin, P. H.; Vioux, A. ^{29}Si Nuclear Magnetic Resonance Study of the Structure of Silicon Oxycarbide Glasses Derived from Organosilicon Precursors. *J. Mater. Sci.* **1995**, *30*, 2313−2318.
(18) Baird, J. D.; Taylor, J. Reaction between Silica and Carbon and the Activity of Silica in Slag Solution. *Trans. Faraday Soc.* **1958**, *54*, 526−539.
(19) Klinger, N.; Strauss, E. L.; Komarek, K. L. Reactions between Silica and Graphite. *J. Am. Ceram. Soc.* **1966**, *49*, 369−375.
(20) Walter, S.; Soraru, G. D.; Bréquel, H.; Enzo, S. Microstructural and Mechanical Characterization of Sol Gel-Derived Si−O−C Glasses. *J. Eur. Ceram. Soc.* **2002**, *22*, 2389−2400.
(21) Bois, L.; Maquet, J.; Babonneau, F.; Bahloul, D. Structural Characterization of Sol-Gel Derived Oxycarbide Glasses. 2. Study of the Thermal Stability of the Silicon Oxycarbide Phase. *Chem. Mater.* **1995**, *7*, 975−981.
(22) Bréquel, H.; et al. Systematic Structural Characterization of the High-Temperature Behavior of Nearly Stoichiometric Silicon Oxycarbide Glasses. *Chem. Mater.* **2004**, *16*, 2585−2598.
(23) Widgeon, S. J.; Sen, S.; Mera, G.; Ionescu, E.; Riedel, R.; Navrotsky, A. ^{29}Si and ^{13}C Solid-State NMR Spectroscopic Study of Nanometer-Scale Structure and Mass Fractal Characteristics of Amorphous Polymer Derived Silicon Oxycarbide Ceramics. *Chem. Mater.* **2010**, *22*, 6221−6228.
(24) Saha, A.; Raj, R.; Williamson, D. L. A Model for the Nanodomains in Polymer-Derived SiCO. *J. Am. Ceram. Soc.* **2006**, *89*, 2188−2195.
(25) Kroll, P. Searching Insight into the Atomistic Structure of SiCO Ceramics. *J. Mater. Chem.* **2010**, *20*, 10528−10534.
(26) Paolo, G.; et al. Quantum Espresso: A Modular and Open-Source Software Project for Quantum Simulations of Materials. *J. Phys.: Condens. Matter* **2009**, *21*, 395502.
(27) Wooten, F.; Winer, K.; Weaire, D. Computer Generation of Structural Models of Amorphous Si and Ge. *Phys. Rev. Lett.* **1985**, *54*, 1392−1395.
(28) Smith, J. V.; Blackwell, C. S. Nuclear Magnetic Resonance of Silica Polymorphs. *Nature* **1983**, *303*, 223−225.
(29) Kroll, P. Modeling Amorphous Ceramic Structures. In *Ceramics Science and Technology*; Wiley-VCH Verlag GmbH & Co. KGaA: Weinheim, 2008; pp 39−69.
(30) Kroll, P. Modelling and Simulation of Amorphous Silicon Oxycarbide. *J. Mater. Chem.* **2003**, *13*, 1657−1668.
(31) Kleebe, H.-J.; Gregori, G.; Babonneau, F.; Blum, Y. D.; MacQueen, D. B.; Masse, S. Evolution of C-Rich SiOC Ceramics. *Z. Metallkd.* **2006**, *97*, 699−709.
(32) Kleebe, H.-J.; Turquat, C.; Sorarù, G. D. Phase Separation in an SiCO Glass Studied by Transmission Electron Microscopy and Electron Energy-Loss Spectroscopy. *J. Am. Ceram. Soc.* **2001**, *84*, 1073−1080.
(33) Perdew, J. P.; Burke, K.; Ernzerhof, M. Generalized Gradient Approximation Made Simple. *Phys. Rev. Lett.* **1996**, *77*, 3865−3868.
(34) Charpentier, T.; Ispas, S.; Profeta, M.; Mauri, F.; Pickard, C. J. First-Principles Calculation of ^{17}O, ^{29}Si, and ^{23}Na NMR Spectra of Sodium Silicate Crystals and Glasses. *J. Phys. Chem. B* **2004**, *108*, 4147−4161.
(35) Devine, R.; Dupree, R.; Farnan, I.; Capponi, J. Pressure-Induced Bond-Angle Variation in Amorphous SiO_2. *Phys. Rev. B* **1987**, *35*, 2560−2562.
(36) Dupree, E.; Pettifer, R. F. Determination of the Si-O-Si Bond Angle Distribution in Vitreous Silica by Magic Angle Spinning NMR. *Nature* **1984**, *308*, 523−525.
(37) Engelhardt, G.; Radeglia, R. A Semi-Empirical Quantum-Chemical Rationalization of the Correlation between SiOSi Angles and ^{29}Si NMR Chemical Shifts of Silica Polymorphs and Framework Aluminosilicates (Zeolites). *Chem. Phys. Lett.* **1984**, *108*, 271−274.
(38) Gladden, L. F.; Carpenter, T. A.; Elliott, S. R. ^{29}Si MAS NMR Studies of the Spin-Lattice Relaxation Time and Bond-Angle Distribution in Vitreous Silica. *Philos. Mag. B* **1986**, *53*, L81−L87.
(39) Mauri, F.; Pasquarello, A.; Pfrommer, B. G.; Yoon, Y.-G.; Louie, S. G. Si-O-Si Bond-Angle Distribution in Vitreous Silica from First-Principles ^{29}Si NMR Analysis. *Phys. Rev. B* **2000**, *62*, R4786−R4789.
(40) Pettifer, R. F.; Dupree, R.; Farnan, I.; Sternberg, U. NMR Determinations of Si-O-Si Bond Angle Distributions in Silica. *J. Non-Cryst. Solids* **1988**, *106*, 408−412.
(41) Soleilhavoup, A.; Delaye, J.-M.; Angeli, F.; Caurant, D.; Charpentier, T. Contribution of First-Principles Calculations to Multinuclear NMR Analysis of Borosilicate Glasses. *Magn. Reson. Chem.* **2010**, *48*, S159−S170.
(42) Thomas, J. M.; Klinowski, J.; Ramdas, S.; Hunter, B. K.; Tennakoon, D. T. B. The Evaluation of Non-Equivalent Tetrahedral Sites from ^{29}Si NMR Chemical Shifts in Zeolites and Related Aluminosilicates. *Chem. Phys. Lett.* **1983**, *102*, 158−162.
(43) Alderman, O. L. G.; Iuga, D.; Howes, A. P.; Pike, K. J.; Holland, D.; Dupree, R. Spectral Assignments and NMR Parameter-Structure Relationships in Borates Using High-Resolution ^{11}B NMR and Density Functional Theory. *Phys. Chem. Chem. Phys.* **2013**, *15*, 8208−8221.
(44) Hung, I.; Howes, A. P.; Parkinson, B. G.; Anupõld, T.; Samoson, A.; Brown, S. P.; Harrison, P. F.; Holland, D.; Dupree, R. Determination of the Bond-Angle Distribution in Vitreous B_2O_3 by ^{11}B Double Rotation (DOR) NMR Spectroscopy. *J. Solid State Chem.* **2009**, *182*, 2402−2408.
(45) Umari, P.; Pasquarello, A. Fraction of Boroxol Rings in Vitreous Boron Oxide from a First-Principles Analysis of Raman and NMR Spectra. *Phys. Rev. Lett.* **2005**, *95*, 137401.
(46) Clark, T. M.; Grandinetti, P. J.; Florian, P.; Stebbins, J. F. Correlated Structural Distributions in Silica Glass. *Phys. Rev. B* **2004**, *70*, 064202.
(47) Mahler, J.; Sebald, A. Deconvolution of ^{29}Si Magic-Angle Spinning Nuclear Magnetic Resonance Spectra of Silicate Glasses Revisited — Some Critical Comments. *Solid State Nucl. Magn. Reson.* **1995**, *5*, 63−78.
(48) Neuefeind, J.; Liss, K. D. Bond Angle Distribution in Amorphous Germania and Silica. *Ber. Bunsenges. Phys. Chem.* **1996**, *100*, 1341−1349.
(49) Ionescu, E.; Papendorf, B.; Kleebe, H.-J.; Poli, F.; Müller, K.; Riedel, R. Polymer-Derived Silicon Oxycarbide/Hafnia Ceramic Nanocomposites. Part I: Phase and Microstructure Evolution during the Ceramization Process. *J. Am. Ceram. Soc.* **2010**, *93*, 1774−1782.
(50) Mera, G.; Navrotsky, A.; Sen, S.; Kleebe, H.-J.; Riedel, R. Polymer-Derived SiCN and SiOC Ceramics - Structure and Energetics at the Nanoscale. *J. Mater. Chem. A* **2013**, *1*, 3826−3836.
(51) Radovanovic, E.; Gozzi, M. F.; Gonçalves, M. C.; Yoshida, I. V. P. Silicon Oxycarbide Glasses from Silicone Networks. *J. Non-Cryst. Solids* **1999**, *248*, 37−48.
(52) Sitarz, M.; Czosnek, C.; Jeleń, P.; Odziomek, M.; Olejniczak, Z.; Kozanecki, M.; Janik, J. F. SiOC Glasses Produced from Silsesquioxanes by the Aerosol-Assisted Vapor Synthesis Method. *Spectrochim. Acta, Part A* **2013**, *112*, 440−445.
(53) Babonneau, F.; Soraru, G. D.; D'Andrea, G.; Dire, S.; Bois, L. Silicon Oxycarbide Glasses from Sol-Gel Precursors. *MRS Online Proc. Libr.* **1992**, *271*, 789−794.
(54) Brus, J.; Kolář, F.; Machovič, V.; Svítilová, J. Structure of Silicon Oxycarbide Glasses Derived from Poly(methylsiloxane) and Poly[methyl(phenyl)siloxane] Precursors. *J. Non-Cryst. Solids* **2001**, *289*, 62−74.
(55) Sorarù, G. D.; D'Andrea, G.; Campostrini, R.; Babonneau, F.; Mariotto, G. Structural Characterization and High-Temperature Behavior of Silicon Oxycarbide Glasses Prepared from Sol-Gel Precursors Containing Si-H Bonds. *J. Am. Ceram. Soc.* **1995**, *78*, 379−387.
(56) Suyal, N.; Hoebbel, D.; Mennig, M.; Schmidt, H. A Solid State ^{29}Si and ^{13}C NMR Study on the Synthesis of Thin Silicon-Oxycarbide Glass Sheets by a Sol-Gel Route. *J. Mater. Chem.* **1999**, *9*, 3061−3067.
(57) Ionescu, E.; Kleebe, H.-J.; Riedel, R. Silicon-Containing Polymer-Derived Ceramic Nanocomposites (PDC-NCs): Preparative Approaches and Properties. *Chem. Soc. Rev.* **2012**, *41*, 5032−5052.

(58) Merkle, A. B.; Slaughter, M. Determination and Refinement of the Structure of Heulandite. *Am. Mineral.* **1968**, *53*, 1120−38.
(59) Olah, G. A.; Hunadi, R. J. Organometallic Chemistry. 17. Silicon-29 and Carbon-13 NMR Spectroscopic Study of Phenylsilyl Anions. The Question of Silicon-Carbon π-π-Electron Delocalization and Comparison with Related Carbanions. *J. Am. Chem. Soc.* **1980**, *102*, 6989−6992.
(60) Elsen, J.; King, G. S. D.; Mortier, W. J. Influence of Temperature on the Cation Distribution in Calcium Mordenite. *J. Phys. Chem.* **1987**, *91*, 5800−5805.
(61) Galli, E.; Gottardi, G. The Crystal Structure of Stilbite. *Mineral. Petrogr. Acta* **1966**, *12*, 1−10.
(62) Varga, T.; Navrotsky, A.; Moats, J. L.; Morcos, R. M.; Poli, F.; Müller, K.; Saha, A.; Raj, R. Thermodynamically Stable $Si_xO_yC_z$ Polymer-Like Amorphous Ceramics. *J. Am. Ceram. Soc.* **2007**, *90*, 3213−3219.

SUMMARY

This work has demonstrated that it is possible to extract data regarding internal geometry within silicon oxycarbide glass from a NMR spectrum of the material. The use of a large library of structures along with DFT-GIPAW-computed ^{29}Si NMR data provides precise data on both the internal structure of SiCO and the NMR signal of each atom present within the models. The model set includes structures with "glassy" or sp^3-hybridized carbon and structures with graphite-like sp^2-hybridized carbon in the form of aromatic ring structures and one-dimensional graphene strips. These features model the "free" carbon phase present within many SiCO samples.

Linear angular correlation functions were developed for each of the tetrahedral centers present in the set of model structures – SiO_4, SiO_3C, and SiO_2C_2. These functions facilitate a direct relation of the ^{29}Si NMR signal to the average of the four Si—O—Si bonding angles surrounding the central Si atom. Using these relationships, it is possible to extract information on the distribution of angles within a sample of SiCO glass from an experimental ^{29}Si NMR spectrum. The structural data extracted using this technique has shown to be as accurate as the neutron and x-ray diffraction data available in the literature[1] for the respective SiCO samples.

This method makes it possible to get some information that diffraction does not allow, such as regarding the free-C to host interface. The differences in the angular correlation functions for silicon bonding to sp^3-hybridized carbon versus silicon bonding to sp^2-hybridized carbon would result in a difference of 5-10 ppm, assuming the same angle indicated by the SiO_4 and SiO_2C_2 peaks. This difference is quite large and would appear clearly in experiment, however these signals are not present in any data presented in the literature. This indicates that there is no significant amount of bonding between sp^2-hybridized carbon and silicon within the

material. Furthermore, some compression of the angle appears (2-3° per carbon bonded to Si) due to the increased ring strain this additional connectivity provides.

Careful analysis of the SiO_4 peak shows a distribution of wide angles appearing in samples with free carbon, even in very low amounts. Similar large angles are found within zeolite materials with large bores and cage-like voids.[2-4] This suggests that similar features may be present within SiCO, specifically at the interface between the glass and the free carbon. Models with somewhat similar features at the nanometer-scale have been proposed in the literature.[5]

Though this work precludes the presence of covalent bonding between silicon and free carbon, this does not imply any alternate explanation. Thus the possibility remains for some other covalent bonding mode to act as a bonding interface between the free carbon phase and the host glass. Such possibilities include Si—O—C bridging or perhaps other, more complex residual structural features from the polymeric or molecular precursors, This work also gives no insight into the $SiOC_3$ or SiC_4 centers, nor of how the NMR shifts of these centers relate to structural variation in the material, as none of these centers exist within the model structure library.

The nature of how the so-called “wide angle” peak is related to the presence of free carbon also remains unclear. Since this works was published, an alternative explanation has come to light – 5-connected SiO_5 centers also show up in NMR in the same region. Though these centers are unstable, it is possible that some small portion of these centers gains “local stability” during the vitrification process. However, it has also been shown that the area underneath this peak directly correlates to the amount of free carbon within the material sample. Therefore, this peak must correlate to free carbon in some way that is not yet clear. Finally, the models this work

is based on are very small (n ≈ 100 atoms). It is impossible to look at nanometer-scale effects in such small models. Far larger models (e.g. with 10,000 to 100,000 atoms) may be required in the future to examine how these materials interact with internal segregation of carbon, and how the carbon segregations form during synthesis.

REFERENCES

1. Umari, P.; Pasquarello, A. Fraction of Boroxol Rings in Vitreous Boron Oxide from a First-Principles Analysis of Raman and NMR Spectra. *Phys. Rev. Lett.* **2005**, 95, 137401.
2. Merkle, A. B.; Slaughter, M. Determination and Refinement of the Structure of Heulandite. *Am. Mineral*. **1968**, 53, 1120−38.
3. Elsen, J.; King, G. S. D.; Mortier, W. J. Influence of Temperature on the Cation Distribution in Calcium Mordenite. *J. Phys. Chem*. **1987**, 91, 5800−5805.
4. Galli, E.; Gottardi, G. The Crystal Structure of Stilbite. *Mineral. Petrogr. Acta* **1966**, 12, 1−10.
5. Varga, T.; Navrotsky, A.; Moats, J. L.; Morcos, R. M.; Poli, F.; Müller, K.; Saha, A.; Raj, R. Thermodynamically Stable $Si_xO_yC_z$ Polymer-Like Amorphous Ceramics. *J. Am. Ceram. Soc*. **2007**, 90, 3213−3219.

Title: First-Principles Calculations and Analysis of 29Si Nuclear Magnetic Resonance Chemical Shifts in Silicon Oxycarbide Ceramics

Author: John P. Nimmo, Peter Kroll

Publication: The Journal of Physical Chemistry C

Publisher: American Chemical Society

Date: Dec 1, 2014

PERMISSION/LICENSE IS GRANTED FOR YOUR ORDER AT NO CHARGE

This type of permission/license, instead of the standard Terms & Conditions, is sent to you because no fee is being charged for your order. Please note the following:

- Permission is granted for your request in both print and electronic formats, and translations.
- If figures and/or tables were requested, they may be adapted or used in part.
- Please print this page for your records and send a copy of it to your publisher/graduate school.
- Appropriate credit for the requested material should be given as follows: "Reprinted (adapted) with permission from (COMPLETE REFERENCE CITATION). Copyright (YEAR) American Chemical Society." Insert appropriate information in place of the capitalized words.
- One-time permission is granted only for the use specified in your request. No additional uses are granted (such as derivative works or other editions). For any other uses, please submit a new request.